Journal of Power Sources 185 (2008) 973–984

Contents lists available at ScienceDirect

Journal of Power Sources

journal homepage: www.elsevier.com/locate/jpowsour

Analysis and control of a hybrid fuel delivery system for a polymer electrolyte membrane fuel cell

Jinglin He*, Song-Yul Choe**, Chang-Oug Hong

Department of Mechanical Engineering, Auburn University Auburn, AL 36832, USA

ARTICLE INFO

Article history:
Received 3 August 2008
Accepted 10 September 2008
Available online 16 September 2008

Keywords:
PEM fuel cell
Control
Ejector
Blower

ABSTRACT

A polymer electrolyte membrane fuel cell (PEM FC) system as a power source used in mobile applications should be able to produce electric power continuously and dynamically to meet the demand of the driver by consuming the fuel, hydrogen. The hydrogen stored in the tank is supplied to the anode of the stack by a fuel delivery system (FDS) that is comprised of supply and recirculation lines controlled by different actuators. Design of such a system and its operation should take into account several aspects, particularly efficient fuel usage and safe operation of the stack.

The exiting unconsumed hydrogen is circulated and reused to increase the efficiency and at the same time maintain the humidity in the anode side of the stack, thereby preventing drying and flooding in the channel which can affect the stack performance. A high pressure difference across a cell between the anode and cathode could cause damage on thin layers of the cell components and water imbalance in the membranes.

In this paper, we analyze a hybrid fuel delivery system that consists of two supply and two recirculation lines. The major components were a pressure regulator, a flow control valve, an ejector, and a blower. These models were developed and connected in order to analyze dynamic behavior of the fuel delivery system. Based on the models, two control strategies, a decentralized classic proportional and integral control and a state feed-back control were designed and optimized to keep a constant pressure in the anode flow channel and a constant ratio of mass flow rates from recirculation to supply lines. The integrated system with the two different controllers was simulated to evaluate its tracking and rejection performance at different references and disturbances.

1. Introduction

Fuel cells are important technologies that must be developed to meet future power generation needs [1]. Applications in fuel cell vehicles have the potential to substantially to reduce emissions and increase engine efficiency [2]. Among the various fuel cell technologies, the polymer electrolyte membrane (PEM) fuel cell will play a major role in the future hydrogen economy [3] and is considered the best candidate to replace the combustion engine because of its capability of high power densities, low operating temperatures, and short start-up time [4].

Hydrogen stored in a tank is highly pressurized in order to increase the volume density of the fuel. By contrast, the pressure of supplying hydrogen in the stack is relatively low; therefore, a pressure drop is necessary to allow the supply of fuel to quickly respond to power demands. In addition, it is desirable for unconsumed hydrogen to be diverted to a supply line to increase the efficiency of fuel usage and performance of water management. These requirements are fulfilled by the fuel delivery system (FDS). Basic functions of the FDS are to regulate the flow rate of hydrogen supplied to the stack and purge both inert gases, migrated nitrogen from the cathode and liquid water residing in the stack. Therefore, a supply line and a purge line are necessary in a fuel delivery system. The supply line allows the hydrogen from the storage to flow into the anode of the fuel cell stack, where the pressure and mass flow rate are regulated. The purge line periodically discharges the hydrogen from the anode and at the same time removes the liquid water and inert gases accumulated in the channel.

A high excessive ratio of hydrogen is generally preferred, which reduces the response time at an increased power demand, improves efficiency, and eases water removal; the latter is particularly advantageous in water management [5,6]. In these studies, the unconsumed fuel exiting at the outlet of the anode flow channel was diverted to a supply line by an extra ejector or blower [5].

* Corresponding author. Tel.: +1 334 844 3328; fax: +1 334 844 3307.
** Corresponding author.
E-mail addresses: hejingl@auburn.edu (J. He), choe@eng.auburn.edu (S.-Y. Choe), cwhong@hyundai-rotem.co.kr (C.-O. Hong).

0378-7753/$ – see front matter © 2008 Elsevier B.V. All rights reserved.
doi:10.1016/j.jpowsour.2008.09.011

Nomenclature

a_w	water activity
A	area (m^2)
c_p	specific heat at constant pressure($J\,kg^{-1}\,K^{-1}$)
C_D	discharge coefficient
d	diameter (m)
F	faraday constant ($96487\,C\,mol^{-1}$)
I	current (A)
J	rotational inertia ($kg\,m^2$)
m	mass (kg)
M	molecular weight ($kg\,mol^{-1}$)
Ma	Mach number
N_{cell}	number of fuel cell
p	pressure (Pa)
R	gas constant ($J\,kg^{-1}\,K^{-1}$)
t	time (s) or thickness (m)
T	temperature (K)
U	speed ($m\,s^{-1}$)
V	volume (m^3)
W	mass flow rate ($kg\,s^{-1}$)
y	mass fraction

Greek letters

α_{net}	net water transfer coefficient
γ	specific heat ratio
η	efficiency
λ	water content
ρ	density ($kg\,m^{-3}$)
τ	torque (N m)
ϕ	relative Humidity
Φ	scaled mass flow rate
Ψ	dimensionless heat parameter
ω	angular velocity ($rad\,s^{-1}$)

Subscription

an	anode
bl	blower
bm	blower motor
ca	cathode
dry	dry state
ej	ejector
em	ejector manifold
fc	fuel cell
fcv	flow control valve
g	mixed gas of hydrogen and vapor
H_2	hydrogen
H_2O	water
in	inlet
l	liquid water
lpr	low pressure regulator
m	membrane
max	maximum
memb	membrane
min	minimum
mix	mixing section of ejector
out	outlet
p	primary flow of ejector
py	primary flow at secondary flow choking section
reacted	reacted hydrogen
ref	reference
s	secondary flow of ejector
sat	saturation
set	setting
sm	supply manifold
st	stack
sy	secondary flow at chocking section
v	vapor
*	steady state

When the load varies dynamically, as is usually found in mobile applications, the FDS should supply the fuel quickly, keeping variation of the pressure in the anode flow channel of the stack to a minimum in order to prevent a potential high pressure difference across the individual cells and subsequent adverse effects on water transport in the membranes [7].

The dynamics of the FDS were studied by several authors using models of components and systems. Pukrushpan [8] proposed a model for a system where a recirculation line and the anode side of the stack were not considered in the study. Bao et al. presented models for a fuel supply line and a recirculation line with an ejector [6], but the recirculation flow rate was not controlled independently because the ejector was in the critical flow condition. Karnik and Sun [7,9], proposed a control-oriented model that considered one supply line and one recirculation line with an ejector to circulate the exiting unconsumed hydrogen. In their study, the recirculation flow was only controlled by the back pressure valve.

We analyzed a new hybrid fuel delivery system that increases efficiency of fuel usage, dynamically supplies the fuel to the stack, and at the same time ensures safe operation of the stack. The FDS consists of two supply and two recirculation lines. The supply lines are operated based on the load demand. At a relatively low load demand, the supply line with a low pressure regulator mainly accounts for the supply of fuel. By contrast, the other line with a flow control valve is used to supply additional flow at a high load demand. An ejector and a blower serve to mix the exiting unconsumed fuel with the supplying flow through two recirculation lines. The ejector is a passive device, while the blower is actively used to control the recirculation flow rate. The control objectives were to maintain the hydrogen stoichiometric ratio (SR) and the pressure difference between anode and cathode using two actuators, a flow control valve and a blower. The schematic diagram of the hybrid FDS is shown in Fig. 1.

The following sections are divided into three parts: description of the models of major components and the hybrid system, steady state analysis of the FDS, and design of controls.

2. Models for components and hybrid system

The hybrid FDS is composed of manifolds, an anode flow channel, an ejector, a blower, a pressure regulator, and a flow control valve. Our modeling (1) assumed no contaminants in the fuel supplied from hydrogen tank and no pressure drops along the pipes, (2) neglected spatial variations, (3) used the ideal gas law for all volumes, (4) assumed isothermal conditions for manifolds and the anode gas flow channel, and (5) assumed that the condensed liquid water in the control volumes is only removed by the purging operation.

2.1. Manifolds

Pipes and connections in the FDS were approximated by two manifolds, an ejector manifold and a supply manifold. The ejector manifold represents the pipe connecting the flow control valve to

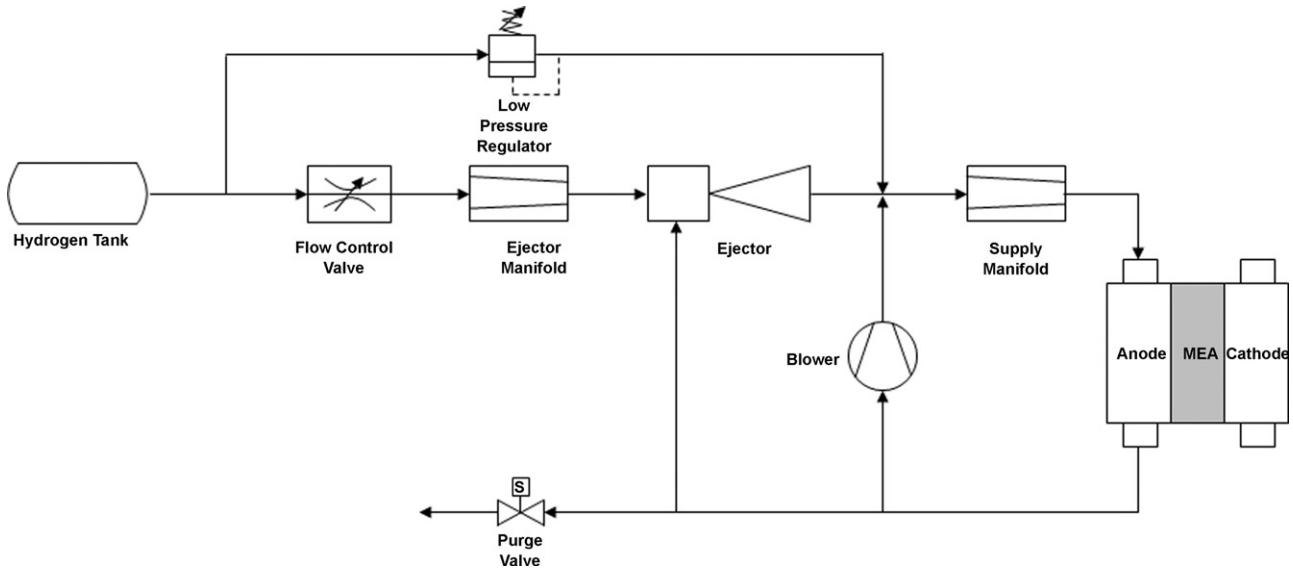

Fig. 1. A hybrid fuel delivery system.

the ejector, and the supply manifold represents the pipe connecting the ejector and blower to the stack.

Because of the assumption that the gas in the ejector manifold is pure hydrogen without contaminants, its pressure dynamics were described by applying the mass conservation law in a control volume;

$$\frac{dp_{em}}{dt} = \frac{R_{H_2} T_{em}}{V_{em}}(W_{fcv} - W_{ej,p}) \tag{1}$$

The inflow of supply manifold includes the recirculation gases from the ejector and the blower, which are a mixed state of hydrogen and water vapor. Using the assumption that no liquid water enters or leaves the supply manifold, the dynamics of the hydrogen and water in the supply manifold are described by;

$$\frac{dp_{H_2,sm}}{dt} = \frac{R_{H_2} T_{sm}}{V_{sm}}(W_{H_2,sm,in} - W_{H_2,sm,out}) \tag{2}$$

$$\frac{dm_{H_2O,sm}}{dt} = W_{v,sm,in} - W_{v,sm,out} \tag{3}$$

When the mass of water in a volume exceeds its saturation limit, liquid water will condenses in it. The mass of saturation water vapor in a volume is determined by;

$$m_{v,sat,(\cdot)} = \frac{p_{sat}(T_{(\cdot)})V_{(\cdot)}}{R_{H_2O} T_{(\cdot)}} \tag{4}$$

where $(\cdot)$ represents the index of volumes with vapor, *sm* and *an*, respectively, referring to the supply manifold and anode flow channel; $m_{v,sat}$ is the saturation mass of water vapor in the volume. p_{sat} is the saturation pressure (Pa), given in the function of volume temperature (K) obtained by curve fitting [10];

$$\log_{10}(P_{sat}(T)) = 1.44 \times 10^{-7} T^3 - 9.18 \times 10^{-5} T^2 + 2.95 \times 10^{-2} T - 2.18 \tag{5}$$

For a volume of hydrogen gas with water vapor and liquid water, the water activity, a_w and humidity, ϕ are defined as [11];

$$a_{w,(\cdot)} = \frac{m_{H_2O,(\cdot)}}{m_{v,sat,(\cdot)}}; \quad \text{and} \quad \phi_{(\cdot)} = \frac{p_{v,(\cdot)}}{p_{sat}(T_{(\cdot)})}; \tag{6}$$

According to the ideal gas law, the water activity is equal to the humidity for sub-saturated vapor in the volume. When the vapor is saturated in the volume, the relationship between the water activity and humidity is given by;

$$\phi_{(\cdot)} = \min(a_{w,(\cdot)}, 1) \tag{7}$$

By substituting Eq. (4) and Eq. (6) into Eq. (3), the dynamics of the water activity are derived as;

$$\frac{da_{w,sm}}{dt} = \frac{R_{H_2O} T_{sm}}{p_{sat}(T_{sm})V_{sm}}(W_{v,sm,in} - W_{v,sm,out}) \tag{8}$$

The species mass flow rates at the inlet and outlet of supply manifold in Eq. (2) and Eq. (8) are determined by the ejector model and anode inlet model. The inlet of the anode flow channel is regarded as a nozzle, and the mass flow rate is calculated by the nozzle equations [11];

$$W_{nozzle} = p_u \Theta(z) \tag{9}$$

where

$$\Theta(z) = \begin{cases} \dfrac{C_D A_t}{\sqrt{RT_u}}(z)^{1/\gamma}\left\{\dfrac{2\gamma}{\gamma-1}(1-(z)^{(\gamma-1)/\gamma})\right\}^{1/2}, & z > \left(\dfrac{2}{\gamma+1}\right)^{\gamma/(\gamma-1)} \\ \dfrac{C_D A_t}{\sqrt{RT_u}}\gamma^{1/2}\left(\dfrac{2}{\gamma+1}\right)^{(\gamma+1)/2(\gamma-1)}, & z \le \left(\dfrac{2}{\gamma+1}\right)^{\gamma/(\gamma-1)} \end{cases} \tag{10}$$

where p_u is the upstream pressure, z the pressure ratio of upstream and downstream, C_D the discharge coefficient of the nozzle, and A_t is the throat area of the nozzle; R and γ are the gas constant and specific heat ratio of the upstream gas.

When applying Eq. (9) and Eq. (10) to the inlet of the anode flow channel, the pressure in the supply manifold is the upstream pressure, the pressure in the anode flow channel is the downstream pressure, and the inlet of the anode flow channel is considered the throat of a nozzle. The average gas constant and specific heat ratio in the supply manifold used in Eq. (10) are defined as;

$$\gamma_{g,(\cdot)} = \gamma_{H_2} y_{H_2,(\cdot)} + \gamma_{H_2O}(1 - y_{H_2,(\cdot)}) \tag{11}$$

$$R_{g,(\cdot)} = R_{H_2} y_{H_2,(\cdot)} + R_{H_2O}(1 - y_{H_2,(\cdot)}) \tag{12}$$

where

$$y_{H_2,(\cdot)} = \frac{p_{H_2,(\cdot)} M_{H_2}}{p_{H_2,(\cdot)} M_{H_2} + p_{sat}(T_{(\cdot)})\phi_{(\cdot)} M_{H_2O}} \tag{13}$$

where y_{H_2} is the mass fraction of hydrogen in the volume, γ_g the average specific heat ratio of humidified hydrogen in the volume based on mass fraction, and R_g is the average gas constant.

2.2. Anode gas flow channel

The anode gas flow channel was considered an isothermal lumped volume with no crossover and leakage. Similar to the manifold models, the pressure and the water activity in the anode flow channel are described as follows;

$$\frac{dp_{H_2,an}}{dt} = \frac{R_{H_2}T_{an}}{V_{an}}(W_{H_2,an,in} - W_{H_2,an,out} - W_{H_2,reacted}) \quad (14)$$

$$\frac{da_{w,an}}{dt} = \frac{R_{H_2O}T_{an}}{p_{sat}(T_{an})V_{an}}(W_{v,an,in} - W_{v,an,out} - W_{v,m}) \quad (15)$$

where $p_{H_2,an}$ is the partial pressure of hydrogen in the anode flow channel. The species mass flow rates entering the channel are expressed as;

$$W_{H_2,an,in} = W_{an,in}y_{H_2,sm}, \quad \text{and} \quad W_{v,an,in} = W_{an,in}(1 - y_{H_2,sm}) \quad (16)$$

where $W_{an,in}$ is the mass flow rate entering anode flow channel derived from Eq. (9) and Eq. (10), and $y_{H_2,sm}$ is the hydrogen mass fraction in the supply manifold.

$W_{H_2,an,out}$ and $W_{v,an,out}$ in Eq. (14) and (15) are the mass flow rates of hydrogen and vapor leaving the anode flow channel, which are derived from the blower and ejector models in the following sections. $W_{H_2,reacted}$ in Eq. (14) is the rate of hydrogen consumed in the electrochemical reaction given by [11];

$$W_{H_2,reacted} = N_{cell}\frac{I_{st}M_{H_2}}{2F} \quad (17)$$

where N_{cell} is number of cells in a stack, I_{st} the stack current and F is Faraday's constant.

$W_{v,m}$ in Eq. (15) is the transport rate of water vapor through the membrane from the anode to the cathode resulting from back diffusions, electro-osmotic drag forces, and pressure gradients along the membrane. The total transport rate of water vapor is given by [12];

$$W_{v,m} = \alpha_{net}N_{cell}\frac{I_{st}M_{H_2O}}{F} \quad (18)$$

where α_{net} is the net water transfer coefficient per proton.

Because of a small pressure gradient across the membrane, the water transport by pressure gradients is negligible, and the net water transfer coefficient is given by [11,12];

$$\alpha_{net} = n_d - \frac{FA_{fc}}{I_{st}}D_w\frac{\rho_{m,dry}}{t_m M_{m,dry}}(\lambda_{ca} - \lambda_{an}) \quad (19)$$

where A_{fc} (cm^2) is the active area, $\rho_{m,dry}$ and $M_{m,dry}$ are the density and the weight per mole of the dry membrane, t_m is the membrane thickness, n_d the electro-osmotic drag coefficient, and D_w is the diffusion coefficient [11];

$$n_d = 0.0029\lambda_{an}^2 + 0.05\lambda_{an} - 3.4 \times 10^{-19} \quad (20)$$

$$D_w = D_\lambda \exp\left(2416\left(\frac{1}{303} - \frac{1}{T_{st}}\right)\right) \quad (21)$$

where D_λ is a diffusion coefficient related to anode water content defined by [12];

$$D_\lambda = \begin{cases} 10^{-10} & \text{for} \quad \lambda_a < 2 \\ 10^{-10}(1 + 2(\lambda_{an} - 2)) & \text{for} \quad 2 \le \lambda_a \le 3 \\ 10^{-10}(3 - 1.67(\lambda_{an} - 3)) & \text{for} \quad 3 \le \lambda_a \le 4.5 \\ 1.25 \times 10^{-10} & \text{for} \quad \lambda_a \ge 4.5 \end{cases} \quad (22)$$

In the above equations, λ_{ca} and λ_{an} are the water contents of the membranes at the cathode and anode sides obtained from the water activity a_w as [11];

$$\lambda_{(\cdot)} = \begin{cases} 0.043 + 17.81a_{w,(\cdot)} - 39.85a_{w,(\cdot)}^2 + 36.0a_{w,(\cdot)}^3 & \text{for} \quad a_{w,(\cdot)} \le 1 \\ 14 + 1.4(a_{w,(\cdot)} - 1) & \text{for} \quad 1 < a_{w,(\cdot)} \le 3 \\ 16.8 & \text{for} \quad a_{w,(\cdot)} > 3 \end{cases} \quad (23)$$

where subscription $(\cdot)$ represents *an* and *ca*, respectively referring to the anode and cathode.

Hence, the transport rate of vapor across the membrane from the anode the cathode was determined at a given stack current and water activities of the flow channels at anode and cathode sides.

One control objective for the FDS is to maintain a specified small pressure difference between anode and cathode and prevent a potential rupture of the membrane. The total pressure in the anode flow channel is calculated by the partial pressures of species as;

$$p_{an} = p_{H_2,an} + p_{sat}(T_{an})\phi_{an} \quad (24)$$

where $\phi_{an} = \min(1, a_{w,an})$ is the relative humidity of gas in the anode flow channel.

2.3. Ejector

Ejectors have been widely applied in refrigerators [13,14]. The same techniques are used in the recirculation systems of the FDS, which allow the low pressure gas exiting from the anode to mix with the high pressure gas in the supply line [7,15,16].

Based on the one-dimensional constant pressure mixing theory and the critical mode, the primary and secondary inlet flows at an ejector are likely to be choked [13]. By Eqs. (9) and (10), the primary and secondary inlet mass flow rates are [7];

$$W_{ej,p} = \frac{p_{em}A_{t,ej}}{\sqrt{T_{em}}}\sqrt{\frac{\gamma_{H_2}}{R_{H_2}}\left(\frac{2}{\gamma_{H_2}+1}\right)^{(\gamma_{H_2}+1)/(\gamma_{H_2}-1)}}\sqrt{\eta_p} \quad (25)$$

$$W_{ej,s} = \frac{p_{an}A_{sy}}{\sqrt{T_{an}}}\sqrt{\frac{\gamma_{g,an}}{R_{g,an}}\left(\frac{2}{\gamma_{g,an}+1}\right)^{(\gamma_{g,an}+1)/(\gamma_{g,an}-1)}}\sqrt{\eta_s} \quad (26)$$

where η_p and η_s are the efficiency for the primary and secondary flow. $A_{t,ej}$ is the nozzle throat area of the ejector, $\gamma_{g,an}$ and $R_{g,an}$ are the average specific heat ratio and gas constant of the anode flow channel, respectively, and A_{sy} is the hypothetical throat area equal to the secondary flow section area where the flow is choked [9], which was determined by;

$$A_{sy} = \begin{cases} A_{mix} - A_{py}, A_{py} < A_{mix} \\ 0, A_{py} \ge A_{mix} \end{cases} \quad (27)$$

where A_{mix} is the mixing tube section area of the ejector and A_{py} is the primary flow section area determined by [13];

$$A_{py} = \frac{A_t}{\eta_{exp}Ma_{py}}\left(\frac{2}{\gamma_{H_2}+1}\left(1 + \frac{\gamma_{H_2}-1}{2}Ma_{py}^2\right)\right)^{(\gamma_{H_2}+1)/[2(\gamma_{H_2}-1)]} \quad (28)$$

$$Ma_{py}^2 = \left(\left(\frac{p_{em}}{p_{rm}}\right)^{(\gamma_{H_2}-1)/\gamma_{H_2}}\left(\frac{\gamma_{g,an}+1}{2}\right)^{(\gamma_{g,an}\gamma_{H_2}-1)/(\gamma_{H_2}\gamma_{g,an}-1)} - 1\right) \times \frac{2}{\gamma_{H_2}-1} \quad (29)$$

where η_{exp} is the coefficient that accounts for loss of primary flow affected at the boundary [13], *Ma* is the Mach number of primary flow at the section where the secondary flow is choked. In addition, the hydrogen and water vapor mass flow rates at the outlet of the ejector are obtained by applying the mass conservation principle;

$$W_{H_2,ej,out} = W_{ej,p} + W_{ej,s}y_{H_2,an} \quad (30)$$

$$W_{v,ej,out} = W_{ej,s}(1 - y_{H_2,an}) \quad (31)$$

where $y_{H_2,an}$ is the hydrogen mass fraction in the anode flow channel calculated by the Eq. (11).

2.4. Blower

A blower used in the recirculation loop allows the humidified hydrogen to circulate from the anode to the supply line. The blower model contains two parts, a blower map and an electric motor. The blower map is used for the static model, which determines mass flow rate and blower efficiency, while the rotational inertia of the electric motor was considered for the dynamics. The blower speed is derived from the model.

The model for the blower assumes that the inlet gas of the blower is the same as that from the return manifold and the blower outlet pressure is equal to that of the supply manifold.

Because the mass flow rate of the blower depends on the inlet gas conditions, the corrected mass flow rate and angle velocity are defined as [17];

$$W_{bc} = W_{bl}\frac{\sqrt{T_{rm}/T_{ref}}}{p_{rm}/p_{ref}}, \quad \text{and} \quad \omega_{bc} = \frac{\omega_{bl}}{\sqrt{T_{rm}/T_{ref}}} \tag{32}$$

where W_{bl} is the mass flow rate of the blower, T_{ref} the reference temperature at 288 (K), p_{ref} the reference pressure of one atmosphere pressure, and ω_{bl} is the blower angle velocity. The dimensionless head parameter Ψ_{bl} is given in [17];

$$\Psi_{bl} = \frac{c_{p,an}T_{an}((p_{sm}/p_{an})^{(\gamma_{g,an}-1)/\gamma_{g,an}} - 1)}{(1/2)U_{bl}^2} \tag{33}$$

where

$$c_{p,an} = c_{p,\mathrm{H}_2}y_{\mathrm{H}_2,an} + c_{p,v}(1 - y_{\mathrm{H}_2,an}) \tag{34}$$

$$U_{bl} = \frac{d_{bl}\omega_{bc}}{2} \tag{35}$$

where $c_{p,an}$ is the average specific heat in the return manifold with a constant pressure of the humidified hydrogen, $c_{p,v}$ and c_{p,H_2} are the specific heats with a constant pressure of water vapor and hydrogen, U_{bl} is the blower rotor tip speed, and d_{bl} is the diameter of blower rotator. The scaled blower flow rate Φ_{bl} is defined by [17];

$$\Phi_{bl} = \frac{W_{bc}}{\rho_{an}\pi/4d_{bl}^2U_{bl}} \tag{36}$$

where

$$\rho_{an} = \frac{p_{an}}{R_{g,an}T_{an}} \tag{37}$$

where ρ_{an} is the gas density in the return manifold. Then, the scaled blower flow rate Φ_{bl} and blower efficiency η_{bl} are expressed as follows [17];

$$\Phi_{bl} = \frac{a_1\Psi_{bl} + a_2}{\Psi_{bl} - a_3}, \quad \text{where} \quad a_i = a_{i1} + a_{i2}Ma, \quad i = 1, 2, 3 \tag{38}$$

$$\eta_{bl} = b_1\Phi_{bl}^2 + b_2\Phi_{bl} + b_3 \quad \text{where} \quad b_i = b_{i1} + b_{i2}Ma, \quad i = 1, 2, 3 \tag{39}$$

$$Ma = \frac{U_{bl}}{\sqrt{\gamma_{g,rm}R_{g,rm}T_{rm}}} \tag{40}$$

where a and b are function parameters, and Ma is the Mach number of the blade tip velocity. The parameters are derived by curve fitting of the experimental data. The calculation results are shown in Table 1.

Based on the static blower map above, the mass flow rate through the blower is given as a function of the pressures and temperatures of inflow and outflow and blower angle velocity, which is derived from the blower motor as [8];

$$\frac{d\omega_{bl}}{dt} = \frac{1}{J_{bl}}(\tau_{bm} - \tau_{bl}) \tag{41}$$

$$\tau_{bl} = \frac{c_{p,rm}T_{rm}}{\omega_{bl}\eta_{bl}}\left(\left(\frac{p_{sm}}{p_{rm}}\right)^{(\gamma_{g,rm}-1)/\gamma_{g,rm}} - 1\right)W_{bl} \tag{42}$$

$$\tau_{bm} = \eta_{bm}\frac{k_t}{R_{bm}}(u_{bl} - k_v\omega_{bl}) \tag{43}$$

where J_{bl} is the rotational inertia of rotator, η_{bm}, k_t, k_v and R_{bm} are motor constants, and u_{bl} is the control voltage of the blower motor.

Table 1
Blower map function parameters.

a	Value	b	Value
a_{11}	-1.598×10^{-3}	b_{11}	-3.20×10^{4}
a_{12}	2.663×10^{-2}	b_{12}	1.51×10^{5}
a_{21}	-3.06×10^{-2}	b_{21}	1.78×10^{2}
a_{22}	-0.174	b_{22}	-1.77×10^{2}
a_{31}	14.6	b_{31}	-2.83×10^{-2}
a_{32}	-15.7	b_{32}	-0.326

2.5. Pressure regulator

The low pressure regulator can adjust its outlet pressure to a setting pressure by manipulating the mass flow rate through an embedded nozzle. The nozzle throat area is varied by the outlet pressure. In this study, a static pressure regulator was used due to short response time. The scaled mass flow rate Φ_{lpr} and the pressure drop Ψ_{lpr} are defined as follows;

$$\Phi_{lpr} = \frac{W_{lpr}}{W_{lpr,\max}}, \quad \text{and} \quad \Psi_{lpr} = \frac{p_{lpr,set} - p_{lpr,out}}{p_{ref}} \tag{44}$$

where W_{lpr} is the mass flow rate through the low pressure regulator, $W_{lpr,max}$ the maximum flow rate, $p_{lpr,set}$ the setting pressure of the regulator, $p_{lpr,out}$ the outlet pressure, and p_{ref} is the reference pressure used for scaling, which is equal to the setting pressure in our model.

By using the curve fitting method, the scaled mass flow rate at the press regulator is approximated with a polynomial as;

$$\Phi_{lpr} = c_1\Psi^3 + c_2\Psi^2 + c_3\Psi + \Phi_{\min,lpr} \tag{45}$$

where $\Phi_{\min,lpr} = W_{lpr,min}/W_{lpr,max}$, and $W_{lpr,min}$ is the minimum controllable mass flow rate. The constants are obtained by a curve fitting method using the experimental data as shown in Table 2.

Because the pressure and temperature of hydrogen tank is regarded as constant, the mass flow rate through the regulator is only a function of the supply manifold pressure (outlet pressure). In addition, it should be noted that the scaled mass flow rate Φ_{lpr} calculated from Eq. (44) becomes saturated at 1.

2.6. Flow control valve

The flow control valve is regarded as a nozzle with a variable throat area, and its steady state behavior is approximated by a linear

Table 2
Constants for the equation used for the low pressure regulator.

Parameter	Value
c_1	-116.1
c_2	29.77
c_3	3.30
$\Phi_{\min,lpr}$	0.077

function of control input signal;

$$W_{fcv} = u_{fcv} W_{fcv,\max} \tag{46}$$

where u_{frv} is the control input signal of the valve that varies from 0 to 1, and $W_{fcv,max}$ is the mass flow rate at the completely opened throat.

3. System analysis

The operation conditions of the hybrid FDS were divided into two modes: low and high loads, each dependent upon the output power of the stack.

In the low load mode, the low pressure regulator line completely supplies the hydrogen consumed by the fuel cell stack, while the flow control valve for the supply line is closed and the ejector recirculation line is out of operation because no fuel is being fed to the primary inlet of the ejector. The blower is the only pump to circulate the excess hydrogen exiting from the anode flow channel. Thus, the operation in the low load was simplified with a pressure regulator and a blower recirculation system. The pressure in the anode flow channel of the stack is maintained by the low pressure regulator and the blower allows adjustment of the hydrogen recirculation flow rate. However, the anode pressure and excess flow could not be simultaneously controlled by one actuator because of the coupled effects between the supply line and the recirculation loop.

In the high load mode, the low pressure regulator alone is not able to meet the fuel requirements for a high output power of the stack. The flow control valve for the supply line begins complementing the additional fuel needed. Both the ejector and the blower are in operation to circulate the excess hydrogen exiting from the anode flow channel, where the pressure in the anode flow channel and hydrogen flow rate in recirculation are controlled by two actuators, the flow control valve and blower. Because of the complexity of the high load mode and its importance in dynamic responses, the following investigations are focused on analysis of the FDS in the high load mode and design of associated controllers.

3.1. Control problem formulation

The dynamic system model of the FDS was obtained by connecting the component models given in Eq. (1)–(46). The model of the FDS includes six state variables: the gas pressure in the ejector manifold, the hydrogen pressures in the supply manifold and anode flow channel, water activities in the supply manifold and anode flow channel, and finally the blower angular velocity. The flow control valve and the blower are the two actuators used for controlling the FDS. The stack current is considered as a disturbance input to the plant. The resulting state equations for the FDS are;

$$\begin{cases} \dot{x} = f(x, u, w) \\ x = (p_{em}, p_{H_2,sm}, a_{w,sm}, p_{H_2,an}, a_{w,an}, \omega_{bl})^T \\ u = (u_{fcv}, u_{bl})^T \\ w = I_{st} \end{cases} \tag{47}$$

where x is the state vector, u the input vector, and w is the disturbance input.

The control objectives of the FDS are to maintain the pressure difference permissible between the anode and cathode and control the hydrogen flow rate for the stack at dynamically varying loads. The hydrogen SR, defined as a ratio of the hydrogen flow rate supplied to that reacted in the anode flow channel was used as a performance variable. Hence, the system output is the anode pressure, and the SR is expressed as follows;

$$\begin{cases} y = g(x, u, w) \\ y = [p_{an}, \mathrm{SR}]^T \end{cases} \tag{48}$$

where y is the output vector, x, u and w are defined in the Eq. (46), p_{an} is the gas pressure in anode flow channel defined in Eq. (16), and $\mathrm{SR} = W_{\mathrm{H_2},an,in}/W_{\mathrm{H_2,reacted}}$.

Because the state equations above are nonlinear, operating points were obtained from steady state analysis, and then the equations were analyzed.

Table 3
Model parameters.

Symbol	Value	Symbol	Value
p_{rc}	1×10^6 Pa	$C_{d,an,in}$	0.95
T_{rc}	293 K	N_{cell}	381
$W_{fcv,max}$	2×10^{-3} kg s^{-1}	V_{an}	5×10^{-3} m^3
V_{em}	4×10^{-3} m^3	T_{an}	353 K
T_{em}	293 K	T_{st}	353 K
$A_{t,ej}$	8.04×10^{-6} m^2	A_{fc}	0.028 m^2
$A_{m,ej}$	4.07×10^{-5} m^2	ρ_m	2×10^3 m^{-3}
η_p	0.88	t_m	5×10^{-4} m
η_s	0.80	M_m	1.1 kg mol^{-1}
η_{exp}	0.70	J_{bl}	2.6×10^{-3} kg m^2
$p_{set,lpr}$	1.5×10^5 Pa	k_t	0.15 N m A^{-1}
$W_{lpr,max}$	1.753×10^{-3} kg s^{-1}	k_v	0.15 V s rad^{-1}
V_{sm}	4×10^{-3} m^3	R_{bm}	0.82 ohm
T_{sm}	353 K	n_{bm}	0.9
$A_{an,in}$	7.5×10^{-5} m^2	d_{bl}	0.15 m

3.2. Analysis at steady state

According to the law of mass conservation at a steady state, the mass flow rate of hydrogen consumed by the stack should be equal to the sum of the two supply lines as;

$$W^*_{\mathrm{H_2},reacted} = W^*_{lpr} + W^*_{fcv} \tag{49}$$

where $W^*_{\mathrm{H_2},reacted}$ is the hydrogen consumption rate at a steady state and as a function of the stack current I_{st}. W^*_{lpr} and W^*_{fcv} are the mass flow rates of the low pressure regulator and flow control valve, respectively.

Because there is no external humidification on the anode side, the membranes of the stack are considered a water source or sink for the FDS system. At a state of equilibrium, the water flow rate cross the membrane should be zero, according to the mass conservation principle. When it is assumed that the membrane at the cathode side is completely humidified in the high load mode, the water content at cathode side becomes the maximum value of 16.8. The water transport across the membrane by back diffusion is balanced by the electro-osmotic drag force. As a result, the net water transfer coefficient becomes zero at steady state. Thus, the corresponding equilibrium water activity in the anode flow channel at a steady state for a given stack current is calculated by setting the net water transfer coefficient to zero in Eq. (19).

A resulting typical I_{st}–$a_{w,an}$ curve at the water equilibrium state is depicted in Fig. 2, and the membrane parameters used in the calculation are listed in Table 3.

As shown in Fig. 2, two different values of the equilibrium water activities in anode flow channel at a given stack current existed; which value results depend upon the previous state. For example, when the stack current is increased from 0 to 400 A, water activity decreases along the line AB, BC and finally the line after C. By contrast, when the stack current is decreased from 400 A to 0, the water activity increases along the line CDA. The liquid water may be condensed in anode flow channel at the low current range of less than about 12 A (dry-out current), where the equilibrium water activity

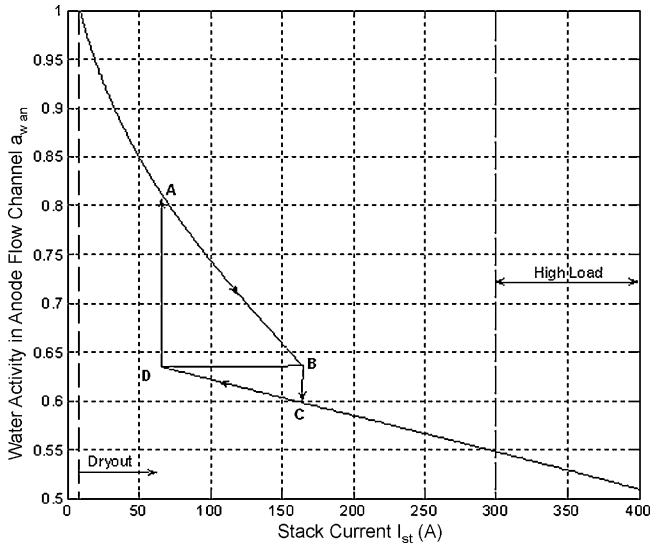

Fig. 2. Water activity versus stack current at water equilibrium.

is larger than 1. When the stack current is larger than the dry-out current, the water activity becomes less than 1, and no liquid water exists in the anode flow channel. In the high load mode, the relationship of water activity and stack current at steady state can be approximated using a linear polynomial.

At a given stack current, values for the state variables and control variables can be obtained by steady state analysis. First, the anode water activity is calculated by the water balance analysis shown in Fig. 2, and the humidity and hydrogen mass fraction in the anode flow channel can be obtained from Eq. (6) and Eq. (13) at the desired pressure in anode flow channel given.

Then, the water vapor mass flow rate leaving the anode flow channel is calculated using the following relationship;

$$W^*_{v,an,out} = W^*_{\mathrm{H}_2,an,out}\frac{1-y^*_{\mathrm{H}_2,an}}{y^*_{\mathrm{H}_2,an}} = (\mathrm{SR}^*-1)W^*_{\mathrm{H}_2,reacted}\frac{1-y^*_{\mathrm{H}_2,an}}{y^*_{\mathrm{H}_2,an}} \tag{50}$$

Because water activity is at a steady state, the water vapor mass flow rate entering the anode flow channel should be equal to that leaving the channel. The mass flow rates entering and leaving the anode flow channel are;

$$W^*_{an,in} = \mathrm{SR}^* W^*_{\mathrm{H}_2,reacted} + W^*_{v,an,out},$$
$$\text{and} \quad W^*_{an,out} = (\mathrm{SR}^*-1)W^*_{\mathrm{H}_2,reacted} + W^*_{v,an,out} \tag{51}$$

Likewise, the hydrogen mass fraction in the supply manifold is obtained by the mass flow rates entering the anode flow channel given by;

$$y^*_{\mathrm{H}_2,sm} = \frac{\mathrm{SR}^* W^*_{\mathrm{H}_2,reacted}}{W^*_{an,in}} \tag{52}$$

In addition, the supply manifold pressure is calculated by the inverted nozzle equations, Eqs. (9) and (10), from the mass flow rate entering the anode channel and hydrogen mass fraction. The mass flow rate of the low pressure regulator is attained by the supply manifold pressure. Both the mass flow rate, W^*_{fcv}, and the control input signal of the flow control valve, u^*_{fcv}, are derived by Eq. (48) and Eq. (45).

At a steady state, the mass flow rate at primary inlet of ejector is equal to that of flow control valve. The pressure of the ejector manifold is derived from Eq. (24). The mass flow rate at the secondary inlet of the ejector, $W^*_{ej,s}$ is obtained by the ejector model in the part 2, which yields the blower mass flow rate;

$$W^*_{bl} = W^*_{an,out} - W^*_{ej,s} \tag{53}$$

The angular velocity of blower was obtained using the inversion of static map of blower in Section 2 by the mass flow rate and the pressure differences of supply manifold and anode flow channel. Thus, the control input u^*_{bl} is determined by the steady state form of Eq. (17) and Eq. (21).

Hence, the reference control variables u^*_{fcv} and u^*_{bl} are a function of control objectives, pressure in the anode flow channel, hydrogen SR, and stack current from the above analysis. Because the pressure in the cathode channel is a function of the stack current, the pressure in anode flow channel also is expressed as a function of the stack current [6]. For an FDS designed for a 100 kW fuel cell stack, the reference pressure in the anode flow channel is given by;

$$p^*_{an} = -0.04583 I^2_{st} - 7.917 I_{st} + 150000 \tag{54}$$

where p^*_{an} is the reference value of the pressure (Pa) in the anode channel, and I_{st} is the stack current in the range of 300–400 A for the high load mode.

The reference hydrogen SR^* is assumed to be 1.5 for different stack currents. Other parameters are given in Table 3.

The operating points of the system were found using tools available in Matlab. Ten different stack currents were selected and the results for the steady state analysis are shown in Fig. 3. As seen in Fig. 3(a) and (b), the control signals for the flow control valve and the blower are nearly linear to the stack current.

The flow rate of consumed hydrogen and the mass flow rates entering and leaving the anode flow channel increases with the increasing stack current. Conversely, the mass flow rate of the low pressure regulator decreases because of the increased pressure in the supply manifold. In addition, the recirculation mass flow rate of the ejector secondary inlet decreases. Consequently, the flow control valve for the supply line becomes the primary fuel supply line and the blower becomes the primary circulation pump for hydrogen recirculation as stack current increased.

As shown in Fig. 3(d), the supply manifold pressure increases and the pressure in the anode flow channel decreases, as defined in Eq. (53), as the stack current increases. In addition, the pressure drop between the inlet and outlet of the anode flow channel increases. Thus, as stack current increases, higher parasitic power is required in the blower, which was dissipated to increase the mass flow rate in the recirculation loops and to overcome the pressure drop along the anode flow channel.

The calculated six state variables of the system at the steady state are shown in Fig. 4. As the stack current increases, the hydrogen partial pressure in the supply manifold increases as shown in Fig. 4(a), and that in the anode flow channel decreases. In addition, water activity in the anode flow channel and in the supply manifold decreases, but activity in the anode flow channel is higher than the other, as shown in Fig. 4(b). The ejector pressure and the blower angle velocity are almost linear to the magnitude of the stack current, as shown in Fig. 4(c) and (d). All the six state variables were determined using a curving fitting method based on the stack current and its relationship given in Fig. 4(a)–(d).

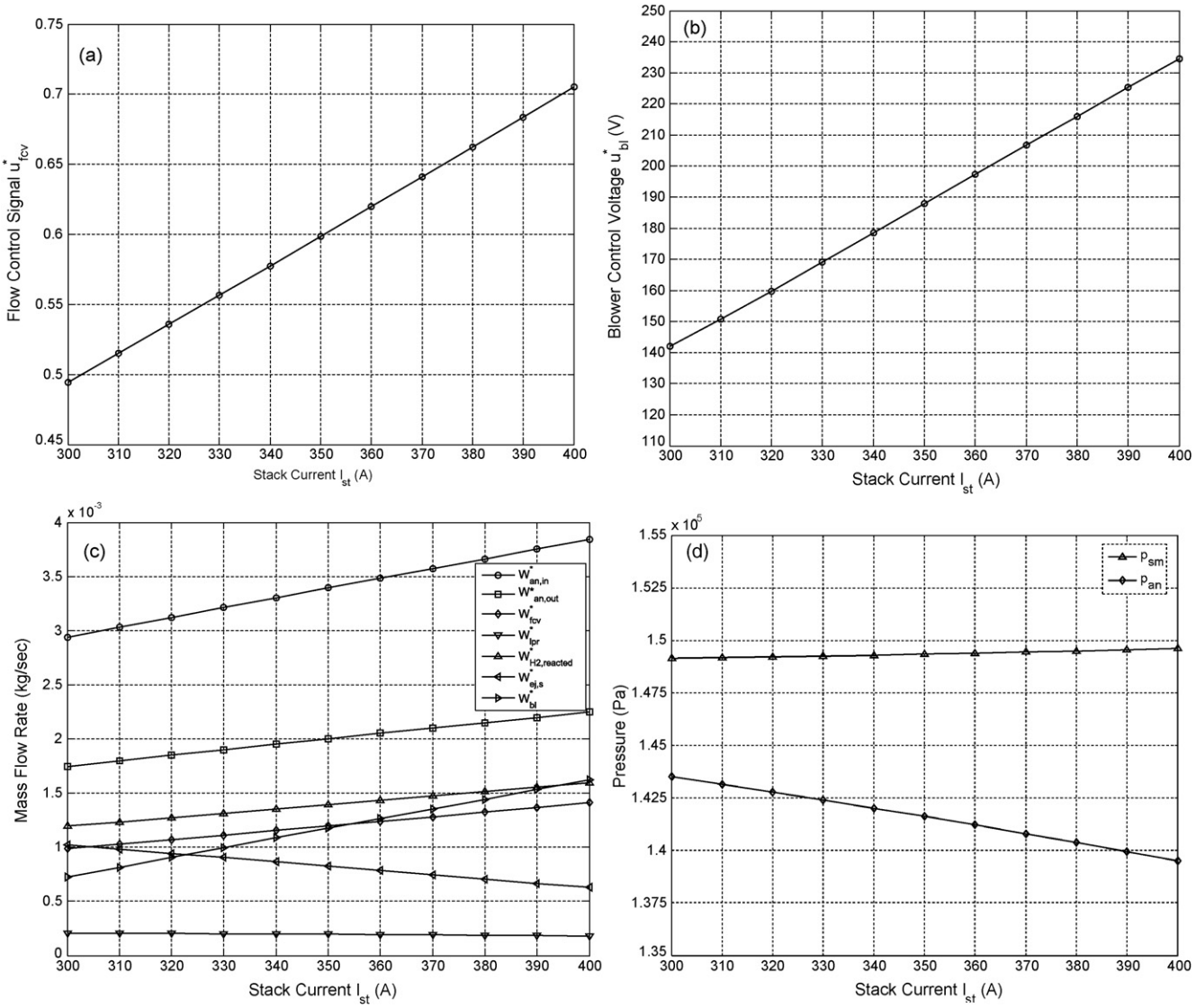

Fig. 3. (a) Reference flow control valve input at a steady state. (b) Reference blower control voltage input at steady state. (c) Mass flow rates at steady state. (d) Pressures at steady state.

3.3. Static feed-forward (SFF)

In the steady state analysis, the reference control variables are expressed as a function of the stack current at a desired anode pressure as given in Eq. (30) and the assumed hydrogen $SR^* = 1.5$. Based on that analysis, the curves in Fig. 3(a) and (b) are approximated by the following two equations used to obtain control signals for the flow control valve and the blower;

$$u^*_{fcv} = 2.108 \times 10^{-3} I_{st} - 0.1391 \tag{55}$$

$$u^*_{bl} = 0.931 I_{st} - 137.9 \tag{56}$$

Based on these equations, a static map was created as a static feed-forward (SFF) block shown in Fig. 5 and used for determining the inputs for the FDS. The outputs are the pressure in the anode flow channel and the hydrogen stoichiometric ratio.

4. Design of linear controller

The SFF had some drawbacks including unexpected disturbances, parameter uncertainties, and approximation errors in the map data that caused deviations in the steady state response. For example, map data that represents the relationship between the voltage for the motor and the mass flow rate is nonlinear. The SFF control of the blower is based on a curve-fitted equation that interpolated the inverse map data. Any change of parameters like aging effects might cause deviations in the characteristic curve for the blower.

Linear feed-back controls are the first choice to avoid instability of the system. For design of the controls, the nonlinear FDS should be linearized at an operating point, which was selected at the stack current, $I_{st} = 350$ A. The resulting control signals for the flow control valve and the blower are 0.59 and 187 V, respectively. The state form of the linearized FDS is;

$$\begin{aligned} \delta\dot{x} &= A\delta x + B_u\delta u + B_w\delta w \\ \delta y &= C\delta x + D_w\delta w \end{aligned} \tag{57}$$

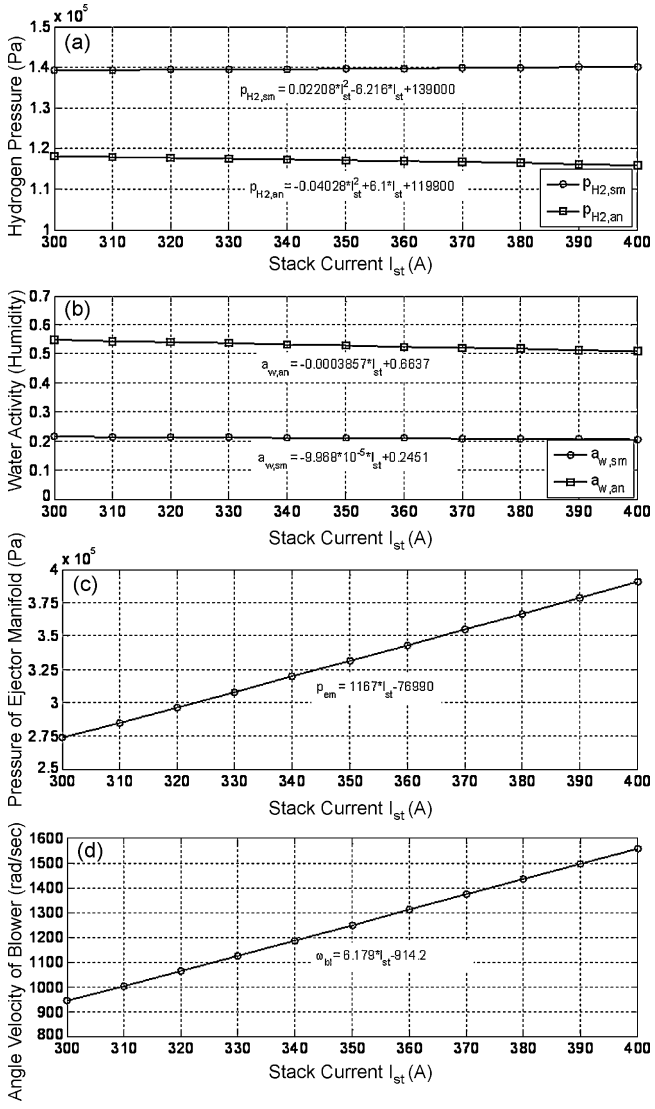

Fig. 4. (a) Hydrogen pressure at steady state. (b) Water activities at steady state. (c) Pressure of ejector manifold at steady state. (d) Angle velocity of blower at steady state.

where $\delta(\,) = (\,) - (\,)_0$ refer to the perturbation from operating points, $(\,)_0$ are the variables at operating points, and A, B_u, B_w, C and D_w are the system matrices.

4.1. Classic proportional integral control

Although the outputs, pressure in anode flow channel, and hydrogen SR are dependent on both inputs, the FDS can be considered as two independent single-input and single-output (SISO) systems, u_{fcv}–p_{an} system and u_{bl}–SR system, to design a diagonal controller as shown in Fig. 6. The use of a diagonal controller for a system with a multi-input and multi-output (MIMO) is referred to as a decentralized controller. Thus, the anode pressure is controlled by the flow control valve, while the hydrogen SR is controlled by the blower.

The decentralized PI controller is implemented by two independent PI controllers, whose transfer function is given as follows;

$$G(s) = k_p + \frac{k_I}{s} \tag{58}$$

where k_p and k_I are the proportional and the integral gains of PI controllers, respectively.

The gains are determined using a design tool given in Matlab for the SISO system. The chosen PI controller gains for u_{fcv}–p_{an} system are $k_{p,pan} = 6.79 \times 10^{-5}$ and $k_{I,pan} = 5.22 \times 10^{-5}\ \mathrm{s}^{-1}$, while those for u_{bl}–SR system are $k_{p,\mathrm{SR}} = 4.58$ and $k_{I,\mathrm{SR}} = 915\ \mathrm{s}^{-1}$.

4.2. State feed-back control

Another feed-back control is state feed-back control with integral, which can stabilize the system by feed-backing outputs and state variables. The resulting full state feed-back control (SFB) with integral is shown in Fig. 7, where two control loops are involved. The inner loop serves to enhance the dynamics of the response by a state feed-back controller, while the outer loop compensates for the steady state tracking error via an integral controller. In addition, the outputs of the SFF are feed-forwarded to the control loop to reduce the transient response time needed for settling to a steady state from a previous state.

Based on the linear model and the block diagram above, the control variable, u, is expressed as a function of the feed-forward output u^*, the perturbation of the state variables δx, and the output of the integrator q;

$$u = u^* - K\delta x - K_I q \tag{59}$$

$$\dot{q} = y^* - y \tag{60}$$

where K and K_I are the state feed-back and integral gain matrices, respectively, and are optimized using the linear quadratic regulator (LQR). The cost function for the LQR is shown as;

$$J = \int_0^\infty (\delta y^T Q_y \delta y + q^T Q_I q + \delta u^T R \delta u)\, dt \tag{61}$$

The cost function includes an output vector, δy, that is a function of the disturbance term, δw, as shown in Eq. (56). To simplify the cost function, a new output vector is defined as;

$$\delta y' = C\delta x \tag{62}$$

Substituting $\delta y'$ to δy in the Eq. (60), the cost function yields a new form;

$$J = \int_0^\infty (\delta x C^T Q_y C \delta x + q^T Q_I q + \delta u^T R \delta u)\, dt \tag{63}$$

The FDS with the controller is depicted in Fig. 7, where the integrator q is considered as a new state variable;

$$\dot{q} = y * -y = -\delta y = -C\delta x - D_w \delta w \tag{64}$$

Neglecting the perturbation of disturbance signal, δw, the expanded state equation integrating Eqs. (56) and (63) is given as;

$$\begin{bmatrix} \delta\dot{x} \\ \dot{q} \end{bmatrix} = \begin{bmatrix} A & 0 \\ -C & 0 \end{bmatrix} \begin{bmatrix} \delta x \\ q \end{bmatrix} + \begin{bmatrix} B_u \\ 0 \end{bmatrix} \delta u = \bar{A} \begin{bmatrix} \delta x \\ q \end{bmatrix} + \bar{B}\delta u \tag{65}$$

The optimization gains of control laws in Eq. (58), which minimize the cost function in Eq. (62) for an infinite period, is given as;

$$[K \quad K_I] = R^{-1}\bar{B}P \tag{66}$$

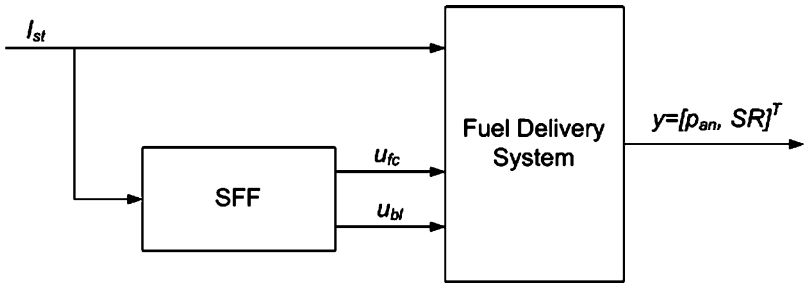

Fig. 5. Static feed-forward control.

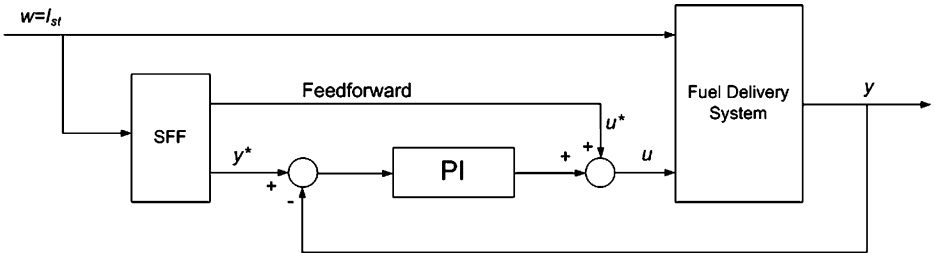

Fig. 6. Decentralized PI controller.

where P is obtained from the solution of the Algebraic Riccati equation;

$$P\bar{A} + \bar{A}^T P + \bar{Q} - P\bar{B}R^{-1}\bar{B}^T P = 0 \tag{67}$$

where

$$\bar{Q} = \begin{bmatrix} C^T Q_y C & \\ & Q_I \end{bmatrix} \tag{68}$$

When the weighting matrices Q_y, Q_I and R are given, the control gains K and K_I are obtained by the LQR algorithm based on the linearization model. Selected Q_y, Q_I and R are as follows;

$$Q_y = \begin{bmatrix} 4\times10^{-6} & \\ & 0.4 \end{bmatrix}, \quad Q_I = \begin{bmatrix} 6\times10^{-5} & \\ & 32 \end{bmatrix},$$

$$R = \begin{bmatrix} 16 & \\ & 4\times10^{-6} \end{bmatrix} \tag{69}$$

Thus, the matrices of the controller gains are computed by solving Eq. (65) and (66) as follows;

$$K = \begin{pmatrix} 2.595\times10^{-1} & 1.293\times10^{-4} & -1.561 & 9.758\times10^{-5} & -2.435\times10^{-5} & 1.865\times10^{-5} \\ -2.591\times10^{4} & -8.401\times10^{-1} & 1.404\times10^{3} & 1.373\times10^{-1} & 3.018 & -1.021\times10^{-2} \end{pmatrix} \tag{70}$$

$$K_I = \begin{pmatrix} -1.234\times10^{-3} & -1.090 \\ 2.984 & -1.803\times10^{3} \end{pmatrix} \tag{71}$$

4.3. Simulation results and analysis

Fig. 8 shows the transient response of the pressure and the hydrogen SR at a step current change. The operating point for the

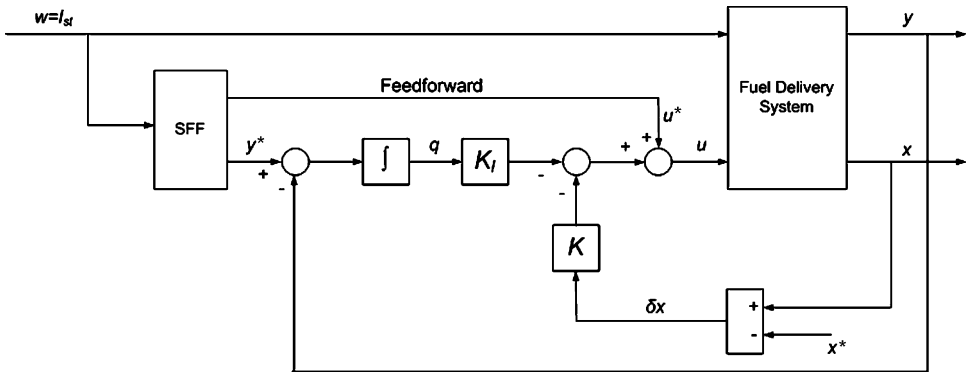

Fig. 7. State feed-back control.

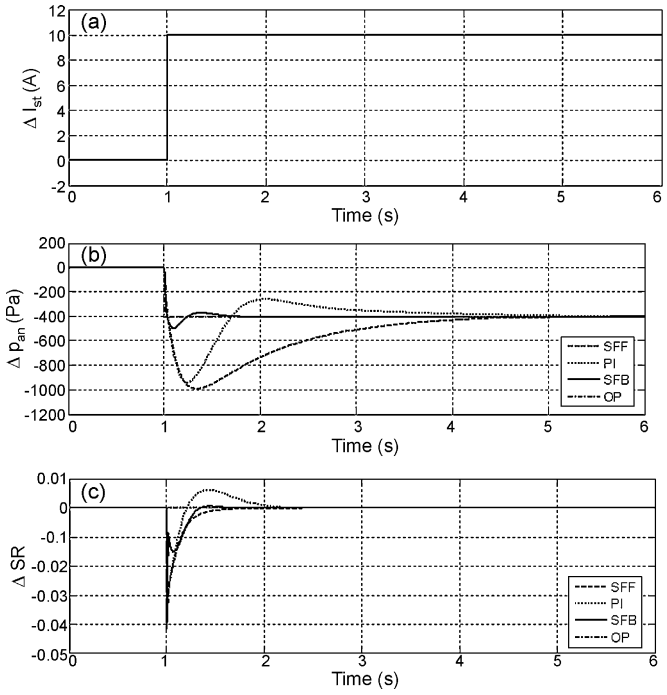

Fig. 8. (a) Step change of stack current. (b) Pressure change in anode flow channel. (c) Hydrogen stoichiometric ratio change.

stack current I_{st} was 350 A, and a current step, $\Delta I_{st} = 10$ A, was applied after 1 s as shown in Fig. 8(a). Fig. 8(b) shows the pressure change responses in the anode flow channel for the three controls. The settle time of the SFB took only about 2 s, while the SFF and PI controls took more than 5 s. The SFF was not able to reach the desired steady state and stayed with an error, while the SFB and PI control followed a reference pressure and finally reached the steady state value.

Similarly, the responses of hydrogen SR change are shown in Fig. 8(c). The settle time at disturbance rejection of the SFB was shorter than that of the SFF and PI control. In addition, the PI control produces a higher overshoot in the SR response than that produced by the SFB, while the SFF control could not remove the steady state error. Consequently, the SFB control outperformed the other controls by its highly dynamic response.

Fig. 9 shows the responses of the FDS at a multi-step stack current that varied from 300 A to 400 A with a period of 5 s as shown in Fig. 9(a). Fig. 9(b) shows the flow control valve signal responses under different control strategies. The control signal of the SFB shows a high overshoot, while it took longer for the PI control to attain a stable state. In addition, the voltage for the blower at the SFB control also had a high overshoot, but the settle time was the shortest, as shown in Fig. 9(c)–(e) show the transient responses of the pressure in the anode flow channel and the hydrogen SR, where the SFB yields the best performance in controlling the pressure and the hydrogen SR. Fig. 9(f) shows the response of the stack current on the water activity in the anode flow channel where no significant differences for the three controls exist. The water activity by all of the controls was smaller than 1 and no liquid water was formed in the flow channel. As a result, no flooding occurred in the anode flow channel at the given multi-step change of stack current in high load, which makes justified the assumption of neglecting purge operation. Because the control requirement for the pressure in the anode flow channel is stricter than that for the hydrogen SR, the SFB is the choice for the FDS.

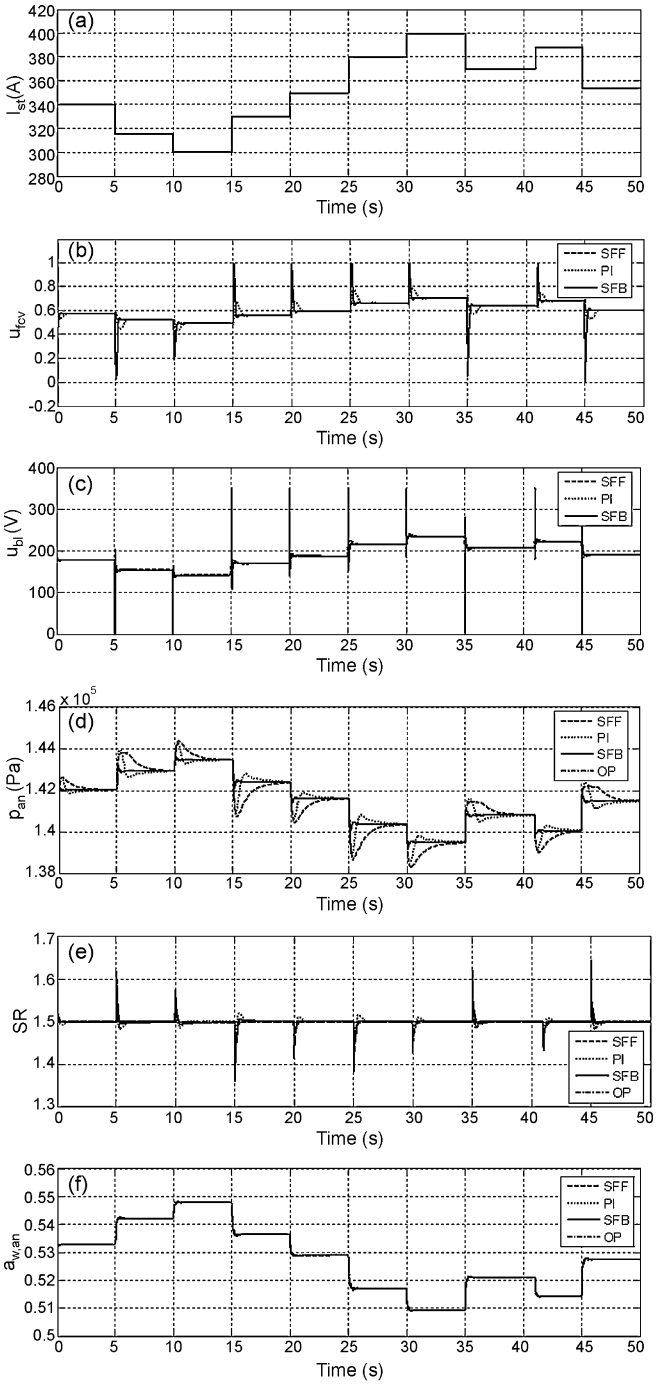

Fig. 9. (a) Multi-step stack current. (b) Flow control valve. (c) Blower control voltage. (d) Anode pressure. (e) Hydrogen stoichiometric ratio. (f) Anode water activity.

5. Conclusion

For this study, we analyzed a hybrid fuel delivery system for a PEM fuel cell power system that was designed to meet requirements of mobile applications. The system consists of two supply and two recirculation lines with an ejector, a blower, and valves that specifically promote efficient, dynamic and reliable operation of the fuel supply. First, models for individual components of the system were developed and used to construct the hybrid system. Based on the models for the system, different control strategies were designed and their performances compared. The major find-

ings of this study are summarized as follows:

1. The conditions for the operation of a hybrid fuel delivery system that depended upon the magnitude of the load current were analyzed. We found that the system could be operated by a low pressure regulator and blower for a low load. The pressure in the anode flow channel and the recirculation mass flow rate were strongly coupled and could not be controlled simultaneously by one actuator in low load mode. By contrast, for a high load, the system needs to be controlled to improve the tracking behavior of the fuel during sudden changes of the stack current. From steady state analysis, both the pressure in anode flow channel and the flow rate of the recirculation were operable by the flow control valve and blower for a high load. Finally, the pressure in anode flow channel and mass flow rate of recirculation could be separately and independently controlled at a high load.
2. According to the comparison of the performance of different control strategies that include the SFF, the PI, and the SFB, the SFB control, based on the linearized model of the FDS, demonstrated the best performance.

The major contributions of this paper are (1) the development of a dynamic model for components of a hybrid fuel delivery system, (2) the design of a decentralized PI controller and a multi-variable linear controller, SFB controller that dynamically controls the recirculation mass flow rate while variation of the pressure in the anode flow channel is suppressed, and (3) the analyses of integrated systems along with their controls.

In real situations, the purging process is necessary to remove inert gases that build up in the recirculation loops as well as the liquid water that forms in the anode flow channel. Effects of the purging process on the performance of FDS will be included in a future study. Measurement of all states is not realistic, so reduction of the states will be carried out using the observer for the SFB control.

Acknowledgments

This research is supported by the Hyundai-Rotem and the author appreciates Mr. C.O. Hong for his help and advice.

References

[1] K. Rajashekara, IEEE Trans. Ind. Appl. 41 (3) (2005) 682–689.
[2] M.B. Stevens, C. Mendes, M. Fowler, R.A. Fraser, 2006 SAE World Congress, Detroit, MI, April 2006.
[3] D. Cheddie, N. Munroe, J. Power Sources 147 (2005) 72–84.
[4] M. Uzunoglu, M.S. Alam, Energ. Conserv. Manage. 48 (2007) 1544–1553.
[5] P. Rodatz, A. Tsukada, M. Mladek, L. Guzzella, Proceeding of the 15th IFAC Triennial World Congress, Barcelona, Spain, July 2002.
[6] C. Bao, M. Ouyang, B. Yi, Int. J. Hydrogen Energy 31 (2006) 1879–1896.
[7] A.Y. Karnik, J. Sun, J.H. Buckland, Proceedings of the American Control Conference, Minneapolis, Minnesota, June 2006.
[8] J.T. Pukrushpan, H. Peng, A.G. Stefanopoulou, J. Dyn. Syst. Meas. Control 126 (2004) 14–19.
[9] A.Y. Karnik, J. S Sun, Proceedings of fuel cell 2005, Third International Conference on Fuel Cell Science Engineering and Technology, Ypsilanti, MI, May 2005.
[10] J. Golbert, D.R. Lewin, J. Power Sources 135 (2004) 135–151.
[11] A.Y. Karnik, A.G. Stefanopoulou, J. Sun, J. Power Sources 164 (2006) 590–605.
[12] S. Dutta, S. Shimpalee, J.W. Van Zee, Int. J. Heat Mass Transfer 44 (2001) 2029–2042.
[13] B.J. Huang, J.M. Chang, C.P. Wang, V.A. Petrenko, Int. J. Refrigeration 22 (1999) 354–364.
[14] G.K. Alexis, Appl. Therm. Engng. 24 (2004) 2657–2663.
[15] F. Marsano, L. Magistri, A.F. Massardo, J. Power Source 129 (2004) 216–228.
[16] Y. Zhu, W. Cai, C. Wen, Y. Li, J. Power Source 173 (2007) 437–449.
[17] P. Moraal, I. Kolmanovsky, International Congress and Exposition, March 1–4, Detroit, MI, 1999.